Plasmon−Phonon Coupling in Charged n-Type CdSe Quantum Dots: A THz Time-Domain Spectroscopic Study

Pankaj K. Mandal and Viktor Chikan*

111 Willard Hall, Department of Chemistry, Kansas State University, Kansas 66506

ABSTRACT

This work aims to experimentally determine the polarizability of confined electron in CdSe quantum dots (QD). The dielectric response of uncharged and charged CdSe quantum dots (3.2 and 6.3 nm) has been measured using terahertz time-domain spectroscopy in the frequency range of 2.0−7.0 THz. A strong coupling between the surface plasmon and surface phonons appears upon charging the QDs. The absolute polarizability of an electron in 3.2 and 6.3 nm charged QDs are experimentally determined to be $0.5 \pm 0.1 \times 10^3$ Å^3 and $14.6 \pm 0.3 \times 10^3$ Å^3, respectively, and the values agree reasonably well with theory and the previous experiment. The observed plasmon−phonon coupling is expected to play an important role in electron relaxation in absence of a hole in CdSe QDs.

Semiconductor nanoparticles are becoming more and more important to technology[1−3] because of their size-tunable optical and electrical properties, which are very different from the bulk semiconductor properties.[4,5] From a fundamental scientific point of view, semiconductor nanoparticles provide a way to study a host of new phenomena related to confined carriers and phonons.[5,6] Tunability of the physical properties of the nanoparticles is mainly the result of the increased surface to volume ratio and the carrier confinement as the size decreases.[7,8] Alternatively, the electrical and optical properties may be manipulated by controlling the carrier concentration in the semiconductor nanoparticles. Controlling the conductivity of the semiconductor nanoparticles is quite important for their application in electro-optic devices[9] such as light-emitting diodes,[10,11] p−n junctions,[12] and solar cells.[13−15] A possible means to control the conductivity is doping the semiconductor nanoparticles with an impurity atom having a different number of valence electrons than the host material. Doping, a very common practice in bulk semiconductor materials, introduces either free electrons (n-type) in the conduction band or free holes (p-type) in the valence band of the semiconductor. Doping a bulk semiconductor increases the carrier density and hence modifies the conductivity. Though doping semiconductor nanocrystals is rather difficult because of self-purification,[16] there have been reports of successful doping of semiconductor quantum dots. For example, Manganese has been successfully doped into several semiconductor nanocrystal systems such as ZnS,[17,18] ZnSe,[19] CdS,[20] and CdSe.[21]

Measuring the conductivity of semiconductor nanoparticles and quantum dots (QDs) is a challenge. Traditional conductivity measurement relies on measurement of current as a function of applied voltage between two electrodes and the sample. Poor electrical connection between the tiny sample and electrodes and the difficulty of characterizing a large number of nanoparticles require an alternative conductivity measurement technique. Terahertz time-domain spectroscopy (THz TDS) has been proven to be a very useful noncontact technique for conductivity measurement of semiconductor nanoparticles.[22,23] The complex refractive index, which is directly related to the complex conductivity of the sample, can be obtained from the THz response. The conductivity measurement by THz TDS yields the ac conductivity of the system, rather than dc conductivity, obtained by traditional conductivity measurements.

CdSe nanocrystals are conveniently synthesized in size ranging from the strong to weak quantum confinement regime and represent an excellent model system to study carrier conductivity. Photoexcited carriers in semiconductor CdSe quantum dots have been studied by several groups;[24,25] an optical pump pulse is used to create an exciton (electron−hole pair), which is subsequently probed in different spectral regimes. In bulk CdSe semiconductor, the carrier energy relaxation is quite fast (sub-ps) and dominated mainly by the Fröhlich interaction with longitudinal optical (LO) phonons.[26] On the other hand, the carrier relaxation (e.g., electronic intraband $1P_e-1S_e$) in CdSe nanocrystals is predicted to be significantly slower due to the so-called "phonon bottleneck", which arises because of quantum confinement that leads to large difference between the

transition energy and the LO phonon energy. However, the studies reviewed in ref 24 and 25 show that the carrier relaxation rate in the nanocrystals is comparable to the bulk relaxation rate and increases with decreasing the size of the nanocrystals. This indicates that the "phonon bottleneck" is not applicable in case of photoexcited CdSe nanocrystals. Further studies demonstrate that the Auger-type electron-to-hole energy transfer and electron−hole Auger recombination are the most likely carrier relaxation pathways.[24,25] A recent study by Hendry et al. provides the first, and only, direct proof of Auger-type electron relaxation.[27] They studied the luminescence upconversion (electron and hole cooling) and transient THz time-domain spectra (hole cooling) of different sizes of photoexcited CdSe quantum dots and estimated the cooling rates for electrons and holes independently.[27] A very recent study reports the state-to-state exciton dynamics in CdSe quantum dots for the first time.[28] Although the carrier dynamics in photoexcited (both electrons and holes are present) nanocrystals are dominated by the Auger processes, the electron relaxation dynamics in absence of a hole is an open question and needs to be studied experimentally and theoretically. To the knowledge of the authors, there is one report by Nozik et al.,[29] where the electron relaxation dynamics have been studied in absence of a hole in chemically charged n-type InP QDs.

There are few other studies on the photoexcited CdSe quantum dots that need to be mentioned here. Schmutten-maer's group has studied the size-dependent photoconductivity of these nanocrystals using time-resolved THz spectroscopy, which used a low-energy THz (0.1−3.0 THz) probe to study the hole dynamics in the valence band.[30] Wang et al. measured the polarizability of the electron−hole pair (exciton), produced by photoexcitation, by studying the change in THz transmission on photoexcitation of very small (1.4−2.4 nm radii (r), strongly quantum confined) CdSe quantum dots.[31] They established an $\sim r^4$ relation of the exciton polarizability and concluded that the hole polarizability is 1 order of magnitude larger than the electron polarizability and contributes mostly towards the total exciton polarizability.[31] A recent similar study supports the previous results in case of CdSe and PbSe QDs.[32]

Although a great deal has been learned about coupled electron−hole dynamics of photoexcited CdSe quantum dots, actual doped CdSe quantum dots are different because only an electron or a hole is present. Guyot-Sionnest and workers have been able to make n-type CdSe nanocrystals by reducing them chemically[33,34] and electrochemically.[35] This paper reports THz time-domain spectroscopic studies of two different sizes (3.2 and 6.3 nm diameter) of chemically charged n-type CdSe quantum dots in the frequency range of 2.0−7.0 THz. Chemical charging introduces one electron to the lowest energy excited state ($1S_e$) of the quantum dots instead of creating an electron−hole pair. Thus, studying these charged n-type quantum dots will yield unambiguous understanding about the electronic contribution toward the polarizability/conductivity (or dielectric response) of excitons in quantum dots and possibly some insight for the electron relaxation dynamics in absence of a hole. Two different sizes

were chosen so that two very different regimes of quantum confinement (strong and weak) are accessible. The Bohr radius (a_B) of CdSe is ∼4.9 nm.[30] The mean diameter of the smaller nanocrystals is 3.2 nm, which is significantly smaller than a_B, whereas the larger particles (mean diameter is 6.3 nm) are larger than a_B. The results also show that the quantum-confined electron can efficiently couple to the Fröhlich mode in charged CdSe QDs.

The THz spectroscopic studies have been carried out using a home-built THz time-domain spectrometer based on a similar design in the literature;[36] see Figure 1a. The spectrometer uses the cavity-dumped output of a mode-locked Ti:sapphire laser (λ_{max} = 780 nm, repetition rate = 2 MHz, average power = ∼80 mW), pumped by a diode laser (532 nm, 4.6 W), for generating and gating the THz radiation. The laser pulse was characterized using a home-built autocorrelator with a GaAsP photodiode as the nonlinear medium.[37] The two-photon nature of the photodiode response was established prior to pulse characterization. The auto-correlation signal of the laser output is shown in Figure 1b. The actual pulse width is $1/\sqrt{2}$ times the width (FWHM of Δt_{auto}) of the autocorrelation signal and is approximately 17.6 ± 0.5 fs in this case if a Gaussian pulse shape is assumed. The ultrafast pulse is negatively chirped to account for the phase dispersion of the optics of the terahertz setup.

As shown in Figure 1a, the IR beam is divided into two parts using a beam splitter. About 75% of the beam (pump beam) is focused onto a 100 μm thick GaP (110) crystal, which generates THz radiation via optical rectification. The diverging THz radiation from the crystal is collected, collimated, and refocused on a second GaP crystal using four gold-coated, off-axis, paraboloidal mirrors. The other 25% of the IR beam (gating beam) is focused on the second crystal for electro-optic (EO) sampling of the THz radiation. The electric field associated with the THz pulse induces a birefringence in the medium of the nonlinear crystal. The gating pulse beam from the EO crystal is passed through a quarter-wave plate and a Wollaston prism, which splits the pulse into two parts with different (vertical and horizontal) polarization. These two beams are fed into two biased photodiodes of a commercially available balanced detector. Any imbalance between the two detector inputs will lead to a net signal. The pre-amplified linear output of the detector is connected to a lock-in amplifier. The pump beam is modulated by using an optical chopper. The amplifier is locked to the chopping frequency, typically 1−2 kHz. The amplified signal is digitized and transferred to a computer for recording and analysis. A delay stage with a typical step size of 3−5 μm is used to vary the delay between the THz pulse and the gating pulse. Hence, the entire THz pulse is mapped out by the gating pulse via electro-optic sampling.

The digitized signal is the electric field of the THz radiation as a function of time. Fourier transform of this time-domain signal yields the amplitude spectrum in the frequency domain. Parts c and d of Figure 1 respectively show the time domain and corresponding frequency domain signals obtained from our spectrometer. The spectrum spans from 0.5 to 8 THz. The signal-to-noise (S/N) ratio is ∼500. The
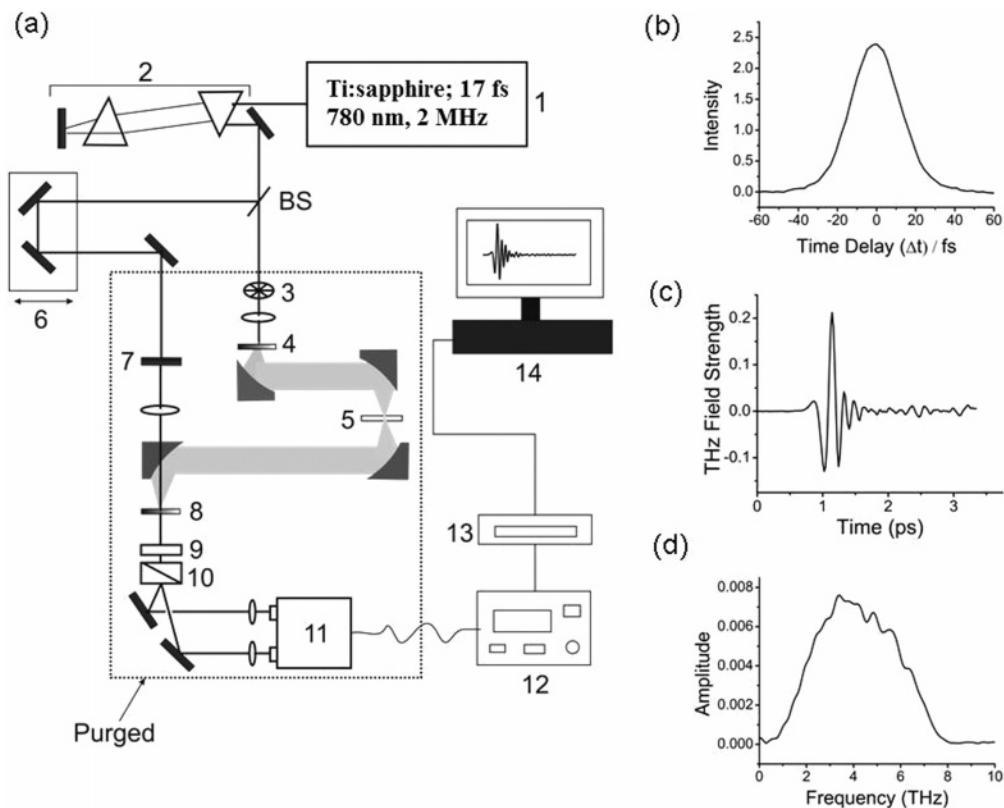
Figure 1. (a) Experimental setup for THz time-domain spectrometer; 1: Ti:sapphire laser with a cavity dumped output of ~17.6 ± 0.5 fs pulse width centered at 780 nm, average power of 80 mW, and a repetition rate of 2 MHz; 2: Prism-pair pulse compressor; 3: Optical chopper, 4: 100 μm thick GaP crystal (THz emitter); 5: Sample; 6: Pulse-delay stage; 7: Polarizer; 8: 100 μm thick GaP crystal (for EO sampling); 9: Quarter-wave plate; 10: Wollaston prism; 11: Balanced detector; 12: Lock-in amplifier; 13: Digitizer; 14: Computer. (b) Autocorrelation signal of the laser light. Actual pulsed width = $\Delta t/\sqrt{2}$ = 17.6 ± 0.5 fs. (c) Measured THz pulse waveform in time domain. (d) Amplitude spectrum (frequency domain) obtained by Fourier transform the THz waveform in (c).

spectral resolution of the present study is approximately 30 cm^{-1} (~1 THz) and is limited by a short scan length. The spectra have been recorded for a short scan length to achieve a good S/N ratio in reasonable time and to avoid reflection from the EO GaP crystal. The entire space and the associated optics covered by the THz light are enclosed with a plexiglass box and purged with dry air/nitrogen to remove water from the THz path. The humidity of the box is continuously monitored by an electronic humidity sensor.

In the present study, all spectral measurements have been carried out from 2.0 to 7.0 THz. The sample is placed at the focal point of the two paraboloidal mirrors (**5** in Figure 1a). To obtain the response of the sample to the THz radiation, two measurements are made. First, the THz electric field transmitted through the empty sample cell ($E_{cell}(t)$) is measured. The sample cell is made of two high resistivity silicon windows (2 mm thick, 1 in. diameter) separated by a Teflon spacer. Next, the THz field transmitted through the cell filled with sample ($E_{sam}(t)$) is recorded. Several measurements, typically 50−100, are averaged to obtain a reasonable S/N ratio. Each measurement takes about 2 min. The shape, amplitude, and the phase of $E_{sam}(t)$ differs from $E_{cell}(t)$ due to the reflection, absorption, and dispersion of THz light by the sample. As the measured signal is the electric field as a function of time, the complex Fourier transform of $E(t)$ will directly yield the complex refractive index of the sample

without Kramers−Kronig analysis. In this work, a windowing function has not been applied to the time-domain signal prior to the Fourier transformation. However, the result would not change even if a windowing function was applied. To extract the complex refractive index of the sample, one needs to take the ratio of the complex Fourier transforms of $E_{sam}(t)$ and $E_{cell}(t)$.

$$\frac{\mathscr{F}E_{sam}(t)}{\mathscr{F}E_{cell}(t)} = \frac{\tilde{E}_{sam}(\omega)}{\tilde{E}_{cell}(\omega)} = \sqrt{T(\omega)}\exp(i\phi(\omega)) \qquad (1)$$

$T(\omega)$ and $\Phi(\omega)$ are the experimentally obtained power transmittance and relative phase, respectively. The complex refractive index ($\tilde{n}(\omega) = n_r(\omega) + in_{im}(\omega)$) of the sample is extracted from the above experimentally obtained quantities using an iterative method following Nashima et al.[38] to account for the Fresnel reflection and transmission losses.

Tri-n-octylphosphineoxide (TOPO) and tri-n-octylphosphine (TOP) capped monodisperse CdSe quantum dots are synthesized using two different routes. The smaller size (3.2 nm) is synthesized from CdO precursor,[39] and the larger size (6.3 nm) is synthesized from Cd(CH$_3$COO)$_2$ precursor.[40] The sizes are determined from the first exciton peak position in the UV−visible spectra of the quantum dots, following the equations derived by Yu et al.[41] Solutions, as concentrated
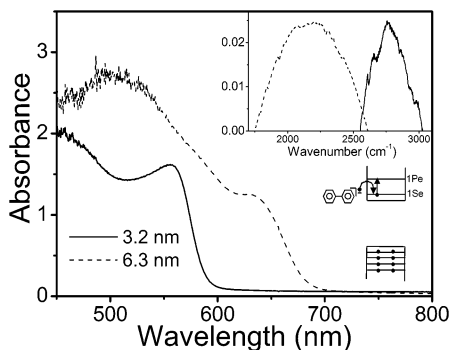
Figure 2. UV−visible spectra of 3.2 and 6.3 nm sized CdSe nanocrystal (uncharged) solutions in HMN. Inset: Infrared absorption spectra showing $1S_e - 1P_e$ transition of the charged n-type CdSe quantum dots.

as possible, of the semiconductor nanocrystals in 2,2,4,4,6,8,8-heptamethylnonane (HMN) are prepared for the THz and IR studies. The n-type semiconductor nanocrystals are prepared by reducing the quantum dots with sodium-biphenyl reagent and metallic sodium.[33] Sodium-biphenyl reagent (50-100 μL, 1.2 M) is added to reduce 2 mL of quantum dot solution. Alternatively, a piece of pure sodium metal is added to the same amount of quantum dot solution and stirred for two weeks. Following Shim et al., a small amount (∼5.0 mg/mL) of TOPO is added to the solution to prevent precipitation of the quantum dots upon charging.[33] Both approaches yield qualitatively similar results. However, only the data using sodium to charge the QDs are presented here.

The sample cell is assembled and the sample is injected into it inside a glove box purged with nitrogen. For the THz measurements of the charged and uncharged quantum dot samples, a cell length (path length) of 1.0 mm is used. The THz response of the solvent (containing the same amount of TOPO as in the QD solutions) is evaluated from the experimental measurements using three different cell lengths (0.2, 0.5, and 1.0 mm). All THz TDS measurements are carried out at room temperature.

As for the previous THz spectroscopic studies of photo-excited CdSe quantum dots,[27,31] the energy of the electromagnetic wave (∼8.0 to ∼29.0 meV) in the present study is much smaller than the lowest energy electronic transitions (∼0.2−0.45 eV) between quantum-confined electron levels. The energy of the terahertz radiation could induce the lowest energy hole transition in the 6.3 nm quantum dots; however, we have assumed that there is no hole in either uncharged or charged quantum dots in both samples. Because some phonon modes are accessible to the high-energy limit of the frequency range of the present study,[42] the dielectric response of the quantum dots to the THz field is expected to be due to a change in electron polarizability at the low-energy limit and due to phonon resonance at the high-energy limit.

The UV−visible absorption spectra of the quantum dot solutions in HMN are shown in Figure 2. As demonstrated previously,[33] the n-type nature of the charged CdSe nanoparticles is established by the appearance of the intraband $1S_e \rightarrow 1P_e$ transition in the infrared spectra, shown as the
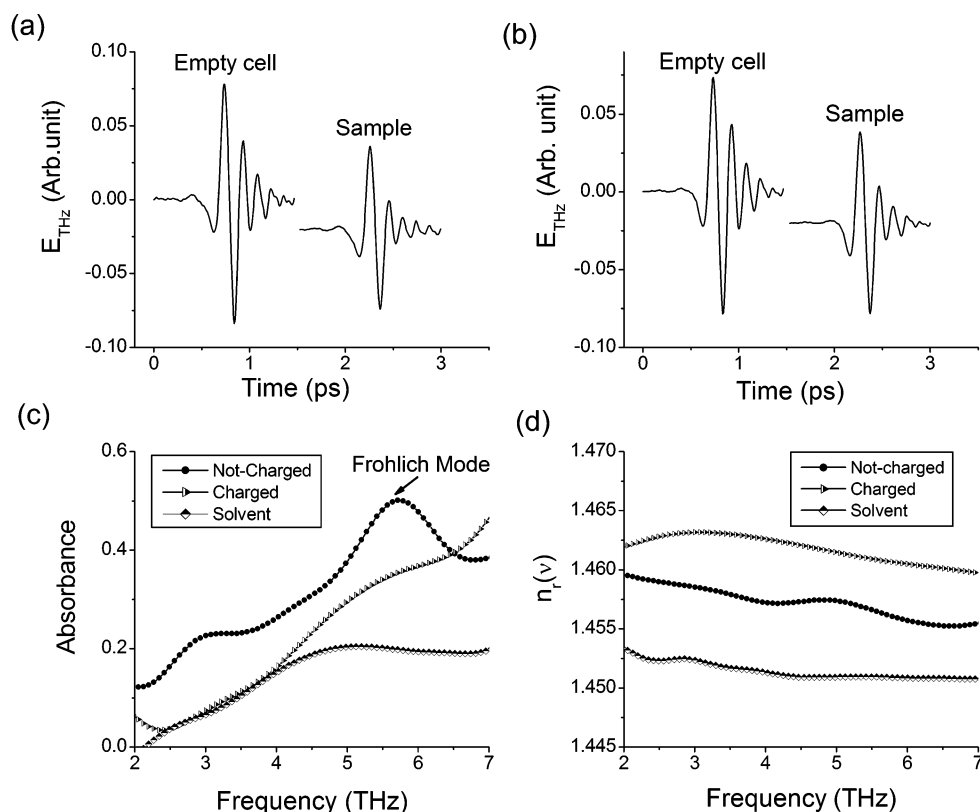
Figure 3. THz TDS measurements of the small (3.2 nm) uncharged and charged CdSe quantum dots. (a) THz waveform measured for the empty sample cell and uncharged quantum dots. (b) THz waveform measured for the empty sample cell and charged n-type quantum dots. (c) Frequency-dependent THz absorbance of the uncharged and charged quantum dots and the solvent obtained from the spectra in (a) and (b). (d) Real refractive indices of the uncharged and charged quantum dots and the solvent.
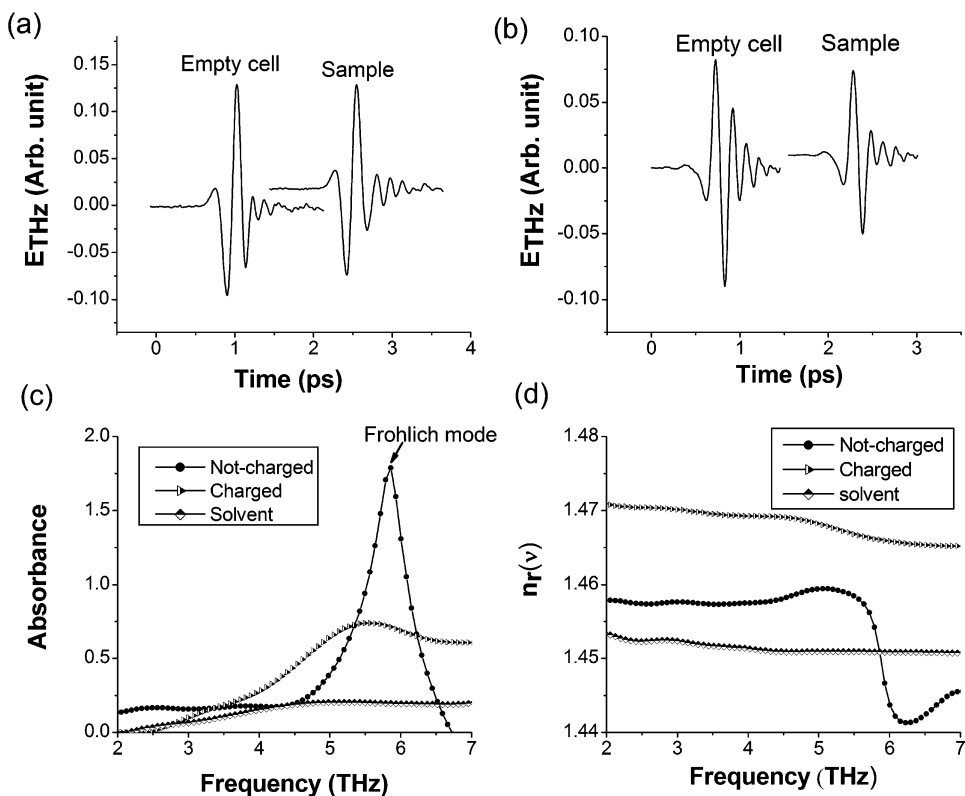
Figure 4. THz TDS measurements of the large (6.3 nm) uncharged and charged CdSe quantum dots. (a) THz waveform measured for the empty sample cell and uncharged quantum dots. (b) THz waveform measured for the empty sample cell and charged n-type quantum dots. (c) Frequency-dependent THz absorbance of the uncharged and charged quantum dots and the solvent obtained from the spectra in (a) and (b). (d) Real refractive indices of the uncharged and charged quantum dots and the solvent.

inset in Figure 2 for both the samples. Figures 3 and 4 show the THz spectroscopic results for both uncharged and charged quantum dots of the 3.2 and 6.3 nm samples, respectively. Figures 3a and 4a show the time-domain THz signals transmitted through the empty cell and the uncharged quantum dot samples of the two sizes, respectively, whereas Figures 3b and 4b are for the charged quantum dots. The change in the amplitude and shape of the THz signal between the cell and the sample is due to the absorption of THz light by the sample. The phase shift of the sample spectra compared to the cell spectra is due to the dispersion of the THz light by the quantum dot solutions. The THz absorbance and the real refractive index of the uncharged and charged quantum dots are extracted by complex Fourier transforms of the time-domain spectra.

The THz absorbance of both uncharged and charged quantum dots are shown in Figures 3c and 4c for 3.2 and 6.3 nm samples, respectively. The absorbance of the solvent is also included in the figures for comparison. The main feature in the THz absorbance spectra of the uncharged quantum dots is a strong resonance at ~5.75 THz (~192 cm^{-1}). This strong absorbance peak is due to a coupled mode between longitudinal optical (LO) phonon and transverse optical (TO) phonon modes, namely the Fröhlich mode, and has been observed earlier in simple far-infrared spectra for small CdSe nanoparticle ensembles.[42] The frequency of this particular mode is size independent. For smaller particles, in addition to the Fröhlich mode, there are some other confined coupled vibrational modes that can be observed in

the THz spectrum as observed in the earlier study.[42] The Fröhlich mode in the small CdSe QD seems less intense and broadened, but this behavior is expected due to mode splitting. However, the low resolution of the present THz measurements prohibits observation of distinct peaks corresponding to each transition. As a result, a broad absorption feature is observed for the small uncharged quantum dots as shown in Figure 3c. For the large particles, only the Fröhlich mode is observed.

There are two interesting differences in the absorbance spectra of the n-type charged quantum dots. First, the Fröhlich transition disappears or diminishes for both samples and a new, broad band appears. The frequency-dependent absorbance for the two charged quantum dot samples are different. For the small CdSe quantum dots, the THz absorbance increases with frequency, and no peak is observed within the frequency range studied. However, the THz absorbance for the larger particles shows a peak at ~5.5 THz.

The real refractive indices ($n_r(\nu)$) for the uncharged and charged nanoparticles are shown in the Figures 3d and 4d for the 3.2 and 6.3 nm samples, respectively. The refractive index of the solvent is also included in the figures. The real refractive index of the solvent is almost constant at a value of ~1.45 in the spectral range of this study. The $n_r(\nu)$ values of the uncharged nanoparticles are slightly higher than that of the solvent. For the small nanoparticles, the refractive index decreases slowly with frequency, having a different nature near the resonance frequencies (Figure 3d). For the large quantum dots, the refractive index does not vary
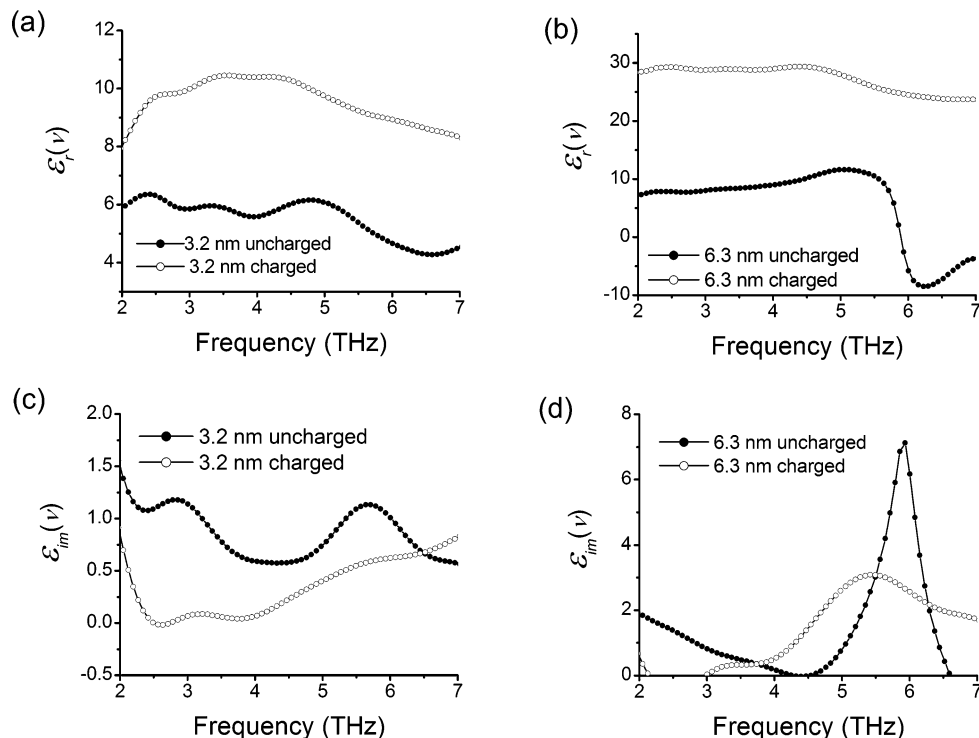
Figure 5. Intrinsic complex dielectric constants of the uncharged and charged quantum dots evaluated from the experimentally obtained effective dielectric constants: (a) and (b) real part and (c) and (d) imaginary part of the complex dielectric constants.

significantly with frequency except for a sudden decrease at the resonance frequency (Figure 4d). The $n_r(\nu)$ values of the charged quantum dots are higher than that of the uncharged ones and decreases slowly with frequency. For the charged 6.3 nm sample, the $n_r(\nu)$ curve shows a relatively sharp change at ~5.5 THz compared to the charged 3.2 nm sample, which is characteristic of a resonance.

The frequency-dependent complex dielectric constants of the charged and uncharged quantum dots have been determined from the experimentally obtained frequency-dependent absorbance and refractive indices. The complex dielectric constant, $\epsilon(\nu)$, is related to the complex refractive index as $\epsilon(\nu) = (n_r(\nu) + in_i(\nu))^2$.[43] The complex dielectric constants obtained from the experimental measurements are the effective dielectric constants of the uncharged and charged quantum dot solutions. The effective dielectric constants have a large contribution from the host medium, which is the solvent. The intrinsic dielectric constants of the uncharged and the charged quantum dots have been evaluated using the simple effective medium approach (EMA)[43]

$$\epsilon_{\text{eff}}(\nu) = f\,\epsilon_i(\nu) + (1 - f)\,\epsilon_h(\nu) \qquad (2)$$

where ϵ_{eff} is the effective complex dielectric constant of the quantum dot solution, and ϵ_i and ϵ_h are the intrinsic complex dielectric constants of the quantum dots and the host medium (solvent), respectively. The use of linear EMA, which assumes no local force induced by neighboring particles acting on the inclusion particle, is justified because the volume fraction ("f" in eq 2) of the quantum dot solutions are quite small (1.3×10^{-3} for small and 2.6×10^{-3} for

large QD solutions). The volume fraction of the inclusion (quantum dots) into the effective medium (solution) is evaluated from the UV−visible spectra of the quantum dot solutions using the known absorption coefficient of the CdSe nanocrystals.[41] The solvent dielectric constant ϵ_h is obtained from THz TDS experiment of the solvent as described in the experimental section.

The real and imaginary parts of the complex dielectric constants of both the charged and uncharged nanocrystals are shown in Figure 5. Parts a and b of Figure 5 show the real dielectric constants of the 3.2 and 6.3 nm samples, respectively. The charged nanocrystals have larger dielectric constants compared to their uncharged counterparts. The increase in real dielectric constant is attributed to the increase in the electron polarizability due to the extra confined electron in the quantum dots.[31] The electron polarizability of the uncharged and charged quantum dots has been evaluated from the low-frequency real dielectric constant values using a simple expression for the molecular polarizability, $\alpha = (\epsilon_r - 1)\epsilon_0/N$, where ϵ_r is the low-frequency real dielectric constant of CdSe quantum dots, ϵ_0 is the static dielectric constant of CdSe, and N is the number of particles per unit volume. Thus, the experimentally determined polarizability values of the charged quantum dots are $1.2 \pm 0.1 \times 10^3$ Å^3 and $18.1 \pm 0.3 \times 10^3$ Å^3 for 3.2 and 6.3 nm samples, respectively. The experimentally determined polarizability values of the corresponding uncharged samples are $0.66 \pm 0.1 \times 10^3$ Å^3 and $3.5 \pm 0.3 \times 10^3$ Å^3, respectively. The difference in polarizability of charged vs uncharged QDs is attributed to the presence of the electron in the quantum confined $1S_e$ level. Consequently, the

calculated polarizability of the quantum confined electron in 3.2 and 6.3 nm QDs are $0.5 \pm 0.1 \times 10^3$ Å^3 and $14.6 \pm 0.3 \times 10^3$ Å^3. The exciton polarizability determined experimentally by Wang et al.[31] is of the order of 10^4 Å^3. They calculated the electron and hole polarizability using a multiband effective-mass model and concluded that the electronic polarizability is an order of magnitude less than the hole polarizability, which contributes mostly toward the exciton polarizability. According to Wang et al., the exciton polarizability depends approximately on the fourth power of the QD radius. On the basis of the experimentally determined polarizability value of a confined electron in 3.2 nm sample, a similar r^4 dependence for the electron polarizability would predict a value of ~10.6×10^3 Å^3 for 6.3 nm sample, which is about 40% smaller than the experimentally determined value. Within the experimental error, the outcome of Wang et al. support the current results reasonably well.

Parts c and d of Figure 5 show the imaginary part of the complex dielectric constants ($\epsilon(\nu)_{im}$) of the 3.2 and 6.3 nm quantum dot samples, respectively. If the dielectric response of the quantum dots (both uncharged and charged) is solely due to polarization, $\epsilon_{im}(\nu)$ is expected to be flat and frequency independent.[31] Instead, different absorption features (see also THz absorbance in Figures 3c,d and 4c,d) are observed for both uncharged and charged quantum dots of both sizes. The absorbance feature of the uncharged quantum dots is mainly governed by the coupled phonon modes, especially the Fröhlich mode. The absorption features of the charged quantum dots are different for the two samples. In both cases, the Fröhlich mode is diminished/disappeared, and a broader feature appears. This absorption cannot be the result of transition between different quantized electronic states in the conduction band because the energy of the electromagnetic field is too small. This absorption feature may arise from the surface plasmon of the charged nanocrystals. The THz absorbance due to the surface plasmon of the singly charged CdSe nanocrystals has been calculated following the simple Drude model for metals,[44] and it is shown in Figure 6 for both samples. The parameters used for this calculation are taken from ref 30. As mentioned earlier, the nature of the broad absorption feature is different for the 3.2 and 6.3 nm charged quantum dots. For the 6.3 nm sample a peak is expected at ~8.0 THz (5.5 THz in the experiment), whereas for the 3.2 nm sample, the absorbance keeps on increasing with frequency within the frequency window studied. The Drude model assumes that the energy levels of the electrons are closely spaced; therefore, this model would not apply in this case because the electronic levels are strongly quantum confined. However, if shallow electron traps exist, there is some viability of the model. Conductivity measurements of strongly quantum confined CdSe nanocrystals indicates that shallow traps are present and do contribute to the dc conductivity of the CdSe nanocrystals.[45,46] Although the calculated THz absorbance curve due to surface plasmon, shown in Figure 6, shows a reasonable resemblance with the experimental observation, the absorbance values of the
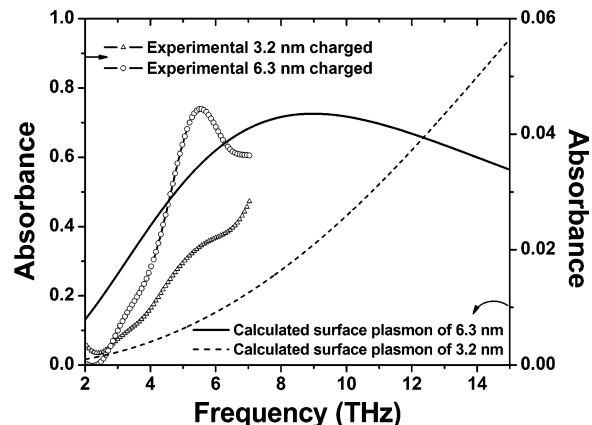
Figure 6. Calculated THz absorption spectra of the singly charged quantum dots of two different sizes due to surface plasmon from the Drude model for metal particles. The experimental THz absorbance of 3.2 and 6.3 nm charged CdSe QD solutions are also included in the plot. The experimental absorbance are about 10 times higher than the calculated surface plasmon modes.

surface plasmon curves are approximately 10 times smaller than the experimental absorbance.

The most probable origin of the broad spectral feature of the charged CdSe nanocrystals is the presence of coupled plasmon−phonon modes. Coupled plasmon−phonon modes have been observed in doped and photoexcited bulk semiconductors.[47−49] Huber et al.[47,48] has investigated the dynamics of the plasmon−phonon coupled modes by time-resolved terahertz spectroscopy in photoexcited InP and GaAs bulk semiconductors. The LO phonon−plasmon coupled modes evolve on the fs time scale and reach quasiequilibrium in ~200 fs. The original narrow LO phonon peak splits into two broad peaks. The broader and stronger peak moves to high frequency and is close to the plasma frequency, whereas the weaker and narrower peak moves below the TO phonon frequency. This coupling occurs through Fröhlich interaction and is important for the carrier relaxation in the bulk semiconductor. The main difference between the result of bulk and quantum confined systems is that the presence of phonon and plasmon is primarily surface phenomenon in the later case. Both of these phenomena have been observed experimentally, and a coupling may exist as for their bulk counterparts. Especially for the 6.3 nm sample, a strong coupling is expected because the Fröhlich mode and surface plasmon mode, predicted from the Drude model, have very close resonance frequencies. The coupling between the surface plasmon and the Fröhlich mode would result in new modes shifted from their original frequencies exhibiting different lifetime broadening. The broad spectral feature of the charged large quantum dots is the result of such a coupling. The strong coupling between these modes would also predict the appearance of a higher frequency mode similar to bulk experiments, but the current experimental setup has a frequency range limited to less than 7−8 THz, depending on the transmission characteristics of the sample. The difference in the dielectric response of the 3.2 and 6.3 nm quantum dots is attributed to the extent of quantum confinement in these systems. The small charged quantum dots exhibit similar features but less pronounced. For the

small quantum dots, the surface plasmon mode, predicted from the Drude model, is expected to shift to higher frequency due to the effective increase in the charge density. The shift in the surface plasmon mode in the small charged quantum dots would yield larger frequency mismatch between the surface plasmon and the Fröhlich mode. The observation of plasmon−phonon coupling in the charged quantum dots indicates that the plasmon−phonon coupling can play a very important role in the phonon-assisted electron relaxation in CdSe nanocrystals in the absence of a hole.

In conclusion, charged n-type CdSe quantum dots of two different sizes, 3.2 and 6.3 nm, have been studied using THz time-domain spectroscopy. The dielectric response of the charged nanocrystals is the combination of electronic polarizability and plasmon−phonon resonance due to an extra electron in the $1S_e$ state. The magnitude of electronic polarizability of the electron in the charged CdSe quantum dots fits well to theory and the previous experiment. Shallow electron traps may play a role in the observed broad feature; however, we believe that the primary reason of the broad terahertz feature is the result of the coupling between the Fröhlich mode and the surface-plasmon mode. Within the limit of the knowledge of the authors, this is the first spectroscopic observation of the coupling between the surface plasmon and Fröhlich mode in quantum confined CdSe nanocrystals. The plasmon−phonon coupling may be a dominant factor in the electron relaxation in the absence of a hole in this nanocrystals system. More systematic experimental and theoretical studies will be carried out to better understand the nature of the broad THz absorption feature of the charged CdSe QDs and its size dependence.

References

(1) Bhattacharya, P.; Ghosh, S.; Stiff-Roberts, A. D. *Annu. Rev. Mater Res.* **2004**, *34*, 1.
(2) Reithmaier, J. P.; Somers, A.; Kaiser, W.; Deubert, S.; Gerschütz, F.; Forchel, O.; Parillaud, O.; Krakowski, M.; Alizon, R.; Hadass, D.; Bilenca, A.; Dery, H.; Mikhelashvili, V.; Eisenstein, G.; Gioannini, M.; Montrosset, I.; Berg, T. W.; van der Poel, M.; Mørk, J.; Tromborg, B. *Phys. Status Solidi B* **2006**, *243*, 3981.
(3) Klostranec, J. M.; Chan, W. C. W. *Adv. Mater.* **2006**, *18*, 1953.
(4) Nirmal, M.; Brus, L. *Acc. Chem. Res.* **1999**, *32*, 407.
(5) Alivisatos, A. P. *Science* **1996**, *271*, 933.
(6) Wang, Y.; Herron, N. *J. Phys. Chem.* **1991**, *95*, 525.
(7) Norris, D. J.; Efros, A. L.; Rosen, M.; Bawendi, M. G. *Phys. Rev. B* **1996**, *53*, 16347.
(8) Norris, D. J.; Bawendi, M. G. *Phys. Rev. B* **1996**, *53*, 16338.
(9) Nozik, A. J. *Annu. Rev. Phys. Chem.* **2001**, *52*, 193.
(10) Alves, M. V.; Semenzato, M. J.; Marega, E.; Gonzalez-Borrero, P. P. *Phys. Status Solidi B* **2002**, *232*, 32.
(11) Colvin, V. L.; Schlamp, M. C.; Alivisatos, A. P. *Nature* **1994**, *370*, 354.
(12) O'Regan, B.; Schwartz, D. T.; Zakeeruddin, S. M.; Gratzel, M. *Adv. Mater.* **2000**, *12*, 1263.
(13) Schaller, R. D.; Klimov, V. I. *Phys. Rev. Lett.* **2004**, *92*.
(14) Oregan, B.; Gratzel, M. *Nature* **1991**, *353*, 737.
(15) Han, L. L.; Qin, D. H.; Jiang, X.; Liu, Y. S.; Wang, L.; Chen, J. W.; Cao, Y. *Nanotechnology* **2006**, *17*, 4736.
(16) Dalpian, G. M.; Chelikowsky, J. R. *Phys. Rev. Lett.* **2006**, *96*, 226802.
(17) Wang, Y.; Herron, N.; Moller, K.; Bein, T. *Solid State Commun.* **1991**, *77*, 33.
(18) Bhargava, R. N.; Gallagher, D.; Hong, X.; Nurmikko, A. *Phys. Rev. Lett.* **1994**, *72*, 416.
(19) Norris, D. J.; Yao, N.; Charnock, F. T.; Kennedy, T. A. *Nano Lett.* **2001**, *1*, 3.
(20) Kanemitsu, Y.; Matsubara, H.; White, C. W. *Appl. Phys. Lett.* **2002**, *81*, 535.
(21) Mikulec, F. V.; Kuno, M.; Bennati, M.; Hall, D. A.; Griffin, R. G.; Bawendi, M. G. *J. Am. Chem. Soc.* **2000**, *122*, 2532.
(22) Schmuttenmaer, C. A. *Chem. Rev.* **2004**, *104*, 1759.
(23) Beard, M. C.; Turner, G. M.; Schmuttenmaer, C. A. *J. Phys. Chem. B* **2002**, *106*, 7146.
(24) Klimov, V. I.; McBranch, D. W.; Leatherdale, C. A.; Bawendi, M. G. *Phys. Rev. B* **1999**, *60*, 13740.
(25) Klimov, V. I. *J. Phys. Chem. B* **2000**, *104*, 6112.
(26) Prabhu, S. S.; Vengurlekar, A. S.; Roy, S. K.; Shah, J. *Phys. Rev. B* **1995**, *51*, 14233.
(27) Hendry, E.; Koeberg, M.; Wang, F.; Zhang, H.; de Mello Donega, C.; Vanmaekelbergh, D.; Bonn, M. *Phys. Rev. Lett.* **2006**, *96*, 057408.
(28) Sewall, S. L.; Cooney, R. R.; Anderson, K. E. H.; Dias, E. A.; Kambhampati, P. *Phys. Rev. B* **2006**, *74*, 235328.
(29) Blackburn, J. L.; Ellingson, R. J.; Micic, O. I.; Nozik, A. J. *J. Phys. Chem. B* **2003**, *107*, 102.
(30) Beard, M. C.; Turner, G. M.; Schmuttenmaer, C. A. *Nano Lett.* **2002**, *2*, 983.
(31) Wang, F.; Shan, J.; Islam, M. A.; Herman, I. P.; Bonn, M.; Heinz, T. F. *Nat. Mater.* **2006**, *5*, 861.
(32) Dakovski, G. L.; Lan, S.; Xia, C.; Shan, J. *J. Phys. Chem. C* **2007**, *111*, 5904.
(33) Shim, M.; Guyot-Sionnest, P. *Nature* **2000**, *407*, 981.
(34) Shim, M.; Wang, C.; Guyot-Sionnest, P. *J. Phys. Chem. B* **2001**, *105*, 2369.
(35) Wang, C.; Shim, M.; Guyot-Sionnest, P. *Science* **2001**, *291*, 2390.
(36) Flanders, B. N.; Arnett, D. C.; Scherer, N. F. *IEEE J. Sel. Top. Quantum Electron.* **1998**, *4*, 353.
(37) Ranka, J. K.; Gaeta, A.; Baltuska, A.; Pshenichnikov, M. S.; Wiersma, D. A. *Opt. Lett.* **1997**, *22*, 1344.
(38) Nashima, S.; Morikawa, O.; Takata, K.; Hangyo, M. *J. Appl. Phys.* **2001**, *90*, 837.
(39) Peng, Z. A.; Peng, X. *J. Am. Chem. Soc.* **2001**, *123*, 183.
(40) Qu, L.; Peng, Z. A.; Peng, X. *Nano Lett.* **2001**, *1*, 333.
(41) Yu, W. W.; Qu, L.; Guo, W.; Peng, X. *Chem. Mater* **2003**, *15*, 2854.
(42) Vasilevskiy, M. I.; Rolo, A. G.; Artemyev, M. V.; Filonovich, S. A.; Gomes, M. J. M.; Rakovich, Yu. P. *Phys. Status Solidi B* **2001**, *224*, 599.
(43) Han, J.; Zhang, W.; Chen, W.; Thamizhmani, L.; Azad, A. K.; Zhu, Z. *J. Phys. Chem. B* **2006**, *110*, 1989.
(44) Mulvaney, P. *Langmuir* **1996**, *12*, 788.
(45) Leatherdale, C. A.; Kagan, C. R.; Morgan, N. Y.; Empedocles, S. A.; Kastner, M. A.; Bawendi, M. G. *Phys. Rev. B* **2000**, *62*, 2669.
(46) Lifshitz, E.; Litvin, I. D. I.; Hodes, G.; Gorer, S.; Reisfeld, R.; Zelner, M.; Minti, H. *Chem. Phys. Lett.* **1998**, *288*, 188.
(47) Huber, R.; Tauser, F.; Brodschelm, A.; Bichler, M.; Abstreiter, G.; Leitenstorfer, A. *Nature* **2001**, *414*, 286.
(48) Huber, R.; Kubler, C.; Tubel, S.; Leitenstorfer, A.; Vu, Q. T.; Haug, H.; Kohler, F.; Amann, M. C. *Phys. Rev. Lett.* **2005**, *94*, 027401.
(49) Hase, M.; Nakashima, S.-i.; Mizoguchi, K.; Harima, H.; Sakai, K. *Phys. Rev. B* **1999**, *60*, 16526.

NL070853Q